Anisotropic Oxidation Resistance in a Ni-Base Single Crystal Superalloy

Fahamsyah H. Latief*, Nashmi H. Alrasheedi

Department of Mechanical Engineering, Al Imam Mohammad Ibn Saud Islamic University (IMSIU),
PO. BOX 5701, Riyadh 11432, Kingdom of Saudi Arabia
*E-mail: fhlatief@imamu.edu.sa

A study on the anisotropic oxidation resistance in a Ni-base single crystal superalloy was investigated at 1000 °C. Overall, the specimens with (100) face showed a higher oxidation rate compared with the specimens with (110) face. These results showed that the anisotropic oxidation resistance occurred in this study. The formation of the oxide scales on the surfaces of superalloy produces a large number of short-circuit diffusion paths. These short-circuit diffusion paths were influenced by the crystallographic orientations during oxidation which finally results in various oxidation rates as a function of the specimen orientations. This anisotropic oxidation resistance can be triggered by the different structure of γ/γ′ interface acting as rapid diffusion paths for cations diffusion during oxidation in the superalloy. Furthermore, the difference in NiO grain size oxides scale structure and the thickness of oxide scale can be used to clarify the oxidation anisotropy in a Ni-base single crystal superalloy.

1. INTRODUCTION

It is well-known that Ni-based single crystal (SC) superalloys have been extensively used for industrial gas turbines components due to their excellence properties in mechanical properties such as creep behavior which are required for materials to be applied at high temperatures [1-3]. Unfortunately, the oxidation process usually occurs while operating at high temperatures. Recently, the operating temperature of gas turbines increases up to above 1000 °C, this results in the materials degradation because of oxidation or corrosion process [4,5].

The oxidation problem is a major problem at high temperature applications. It has to be taken into consideration to improve the durability of the gas turbines components during service at high temperatures. Therefore, the oxidation resistance of materials becomes one of critical factors to assess the lifetime of the gas turbine components. With respect to the oxidation resistance of the SC superalloys, the addition of rhenium has been successfully improved the oxidation resistance including a good local hot corrosion resistance of the SC superalloys as reported by Czech et al. [6]. Sometimes, aluminium and chromium are also added into the SC superalloy to optimize the oxidation behavior and corrosion resistance.

One of most interesting issues in the SC superalloys is related to the effect crystallographic orientation on the properties of the SC superalloys. The difference in mechanical properties or oxidation resistance of the SC superalloys is termed as anisotropy phenomenon. Some works were reported that the mechanical properties of the SC superalloys have been influenced by the crystallographic orientation of the specimens [7,8]. Khoi et al. [9] and Doychak et al. [10] investigated that the crystallographic orientation effect not only affected the mechanical properties but also the oxidation behavior of SC superalloys [9] and the NiAl alloys [10]. Yuan et al. [11] also studied the effect of crystallographic orientation on oxidation behavior of the SC superalloys, however, there was not enough information its mechanism. Therefore, the present study aims to investigate and elaborate the mechanism of oxidation resistance in a SC superalloy in different surface orientations. The microstructures of the specimens before and after isothermal oxidation were also observed to recognize the anisotropic oxidation resistance phenomena in a SC superalloy.

2. EXPERIMENTAL DETAILS

In this study, a SC superalloy with a cylindrical rod is directionally solidified in [001]-direction. The composition of the SC superalloy was 5.74 Al, 0.73 Ti, 6 Cr, 9.3 Co, 1.4 Hf, 3.4 Ta, 2.9 Re, 8.3 W, 0.005 Zr, 0.016 B, 0.019 Fe, 0.07 C and balance Ni (in mass%) was used as an experimental material. SC superalloy was solution heat-treated at 1274 °C for 8 h under argon environment and subsequent by a two-step aging treatment performed by primary aging of 4 h at 1080 °C and secondary aging of 20 h at 871 °C, continued with air cooling to room temperature. Laue X-ray diffraction method was used to analyze the orientation of SC superalloy. The specimens with two different oriented faces, (100) and (110) were prepared in a rectangular shape with the length of 10 mm, width of 4 mm, and thickness of 3.5 mm. The specimens were mechanically polished and cleaned by acetone. The specimens were then ultrasonically cleaned in alcohol and dried in air prior to oxidation tests.

Isothermal oxidation tests were taken place in a tube furnace at 1000 °C for 500 h in air environment. The mass gain of the specimens was quantified discontinuously after oxidation for 25, 50, 100, 200, and 500 h to calculate its oxidation kinetics. The oxide products of SC superalloy after oxidation tests were evaluated by X-ray diffraction using Cu Kα radiation. Meanwhile, the initial microstructure, surface morphology and cross-section of the SC superalloy after oxidation were

analyzed by a scanning electron microscope equipped with energy-dispersive X-ray spectroscopy (EDS).

3. RESULTS

3.1. Oxidation kinetics

Figure 1 shows the square of the specific mass change as a function of oxidation time for a Ni-base SC superalloy at 1000 °C. The curve of the square of mass change presented a nearly linear line, indicating the oxidation kinetics followed a parabolic oxidation law at 1000 °C. The parabolic rate constant (k_p) of the SC superalloy can be estimated by a linear least-squares algorithm [12,13]. The k_p values are 6.3 x 10^{-7} $mg^2cm^{-4}s^{-1}$ on the (100) face and 4.2 x 10^{-7} $mg^2cm^{-4}s^{-1}$ on the (110) face. Briefly, the difference in oxidation rate was apparent even its difference is very small which indicates the anisotropic oxidation resistance occurred in a SC superalloy.
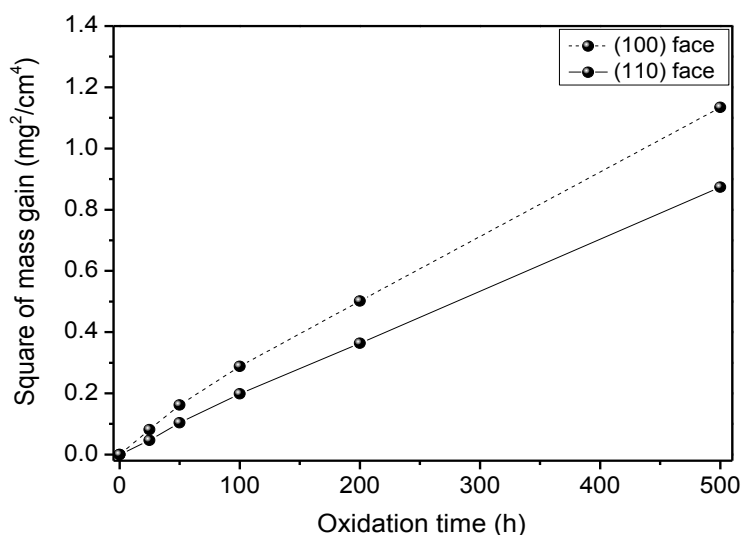

Figure 1. Curve of square of the mass gain per unit area vs oxidation time for SC superalloy after oxidation at 1000°C.

3.2. X-ray diffraction

Figure 2 shows the results of X-ray diffraction of SC superalloy after oxidation at 1000 °C for 500 h. Generally, the oxide scale formed on the surface of SC superalloy between the two surfaces is totally different. Generally, the oxide scale predominantly composed of α-Al_2O_3, followed by $(Ni,Co)O$, spinels $(Ni,Co)Al_2O_4$, Ni_2CrO_4 and $CrTaO_4$. Moreover, some little amounts of $NiTiO_3$, $W_{20}O_{58}$ as well as HfO_2 were also detected after 500 h oxidation at 1000 °C. However, the formation of α-Al_2O_3 was obviously seen in both surface orientations but it can be distinguished from the peaks distinction between the two faces.
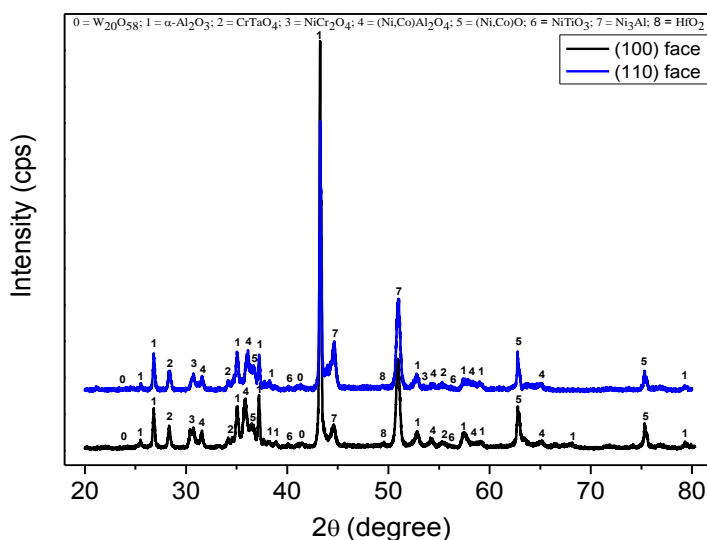
Figure 2. XRD patterns of SC superalloy after 500 h oxidation at 1000°C.

3.3. Microstructure before oxidation

Figure 3 shows the regular cuboidal γ' phase embedded coherently in the γ matrix phase. The SC superalloy used in this study contains 70% volume fraction of the γ' phase. Indeed, the γ/γ' interface configuration is distinct between the two surfaces where its arrangement presented as plus-like on the (100) face and cross-like on the (110) face (Fig. 3).
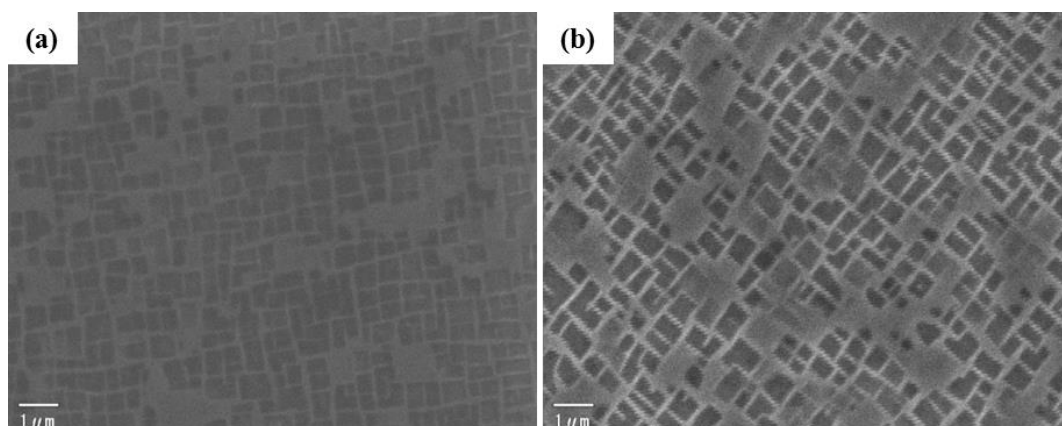

Figure 3. SEM micrographs of SC superalloy for: (a) (100) face and (b) (110) face.

3.4. Surface morphology

Figure 4 shows the surface morphologies of SC superalloy after oxidation for 500 h at 1000 °C. It presents that NiO particles became larger with increasing the oxidation time. The grain size of NiO particles was varied between 0.75-6.8 μm on the (100) face (Fig. 4a), and 0.57-6.15 μm on the (110)

face (Fig. 4b). The oxide scale formed on the surface of SC superalloy after 500 h oxidation at 1000 °C were primarily NiO which has a blocky morphology (typical NiO morphology) [14] with a small amount of CoO for the two surfaces according to the EDS analysis results (Table 1).
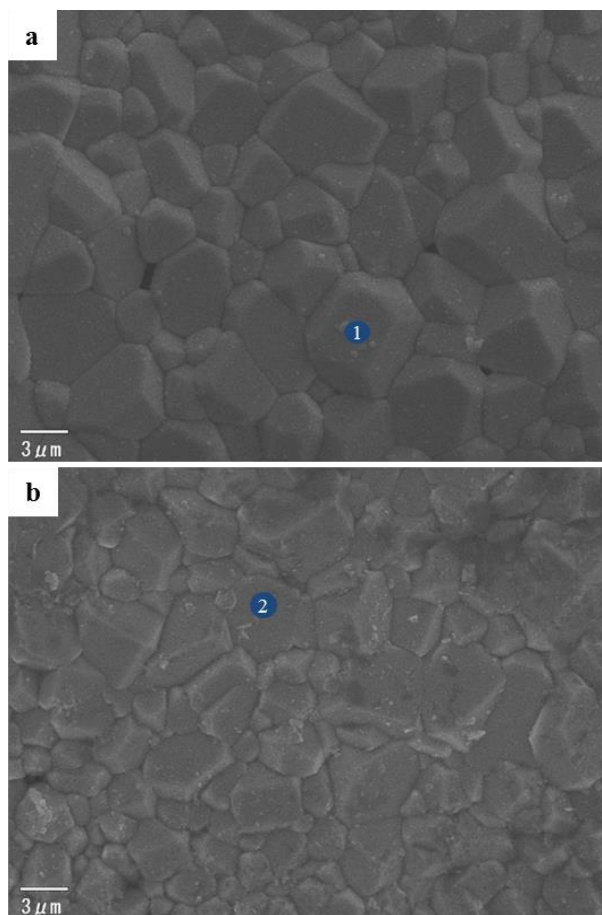

Figure 4. Surface morphologies of SC superalloy after 500 h oxidation at 1000°C for: (a) (100) face and (b) (110) face. The chemical composition of points 1 and 2 are presented in Table 1.

Point 1 in Fig. 4a refers to the (100) face, whereas point 2 in Fig. 4b refers to the (110) face. The content of gold (Au) was detected through the EDS analysis (Table 1) since the specimens were treated by the gold coating prior to the EDS analysis.

Table 1. Chemical content of main elements in the oxide products formed on the SC superalloy.

Specimen orientation	Points of no	Element content (in at%)				Note
		O	Ni	Co	Au	
(100)	1	24.23	62.09	6.73	6.95	NiO + CoO
(110)	2	30.64	58.33	4.21	6.82	NiO + CoO

3.5. Microstructure after oxidation

Figure 5 shows SEM micrographs of the cross-sectional back-scattered electron image (BEI) combined with EDS of the scale formed on the surface of SC superalloy after 500 h oxidation at 1000 °C for both surfaces. The oxide products formed on both surfaces seemed to be similar but different in the configurations on both surfaces. In general, the oxide scales on both surfaces consisted of an outer layer was made of NiO layer with a small amount of CoO (point 1), an intermediate layer (points 2 and 3) and inner layer was composed of continuous α-Al_2O_3 layer which is seen as a dark areas at the bottom of oxide scale combined with a small amount of HfO_2 precipitates (point 4).
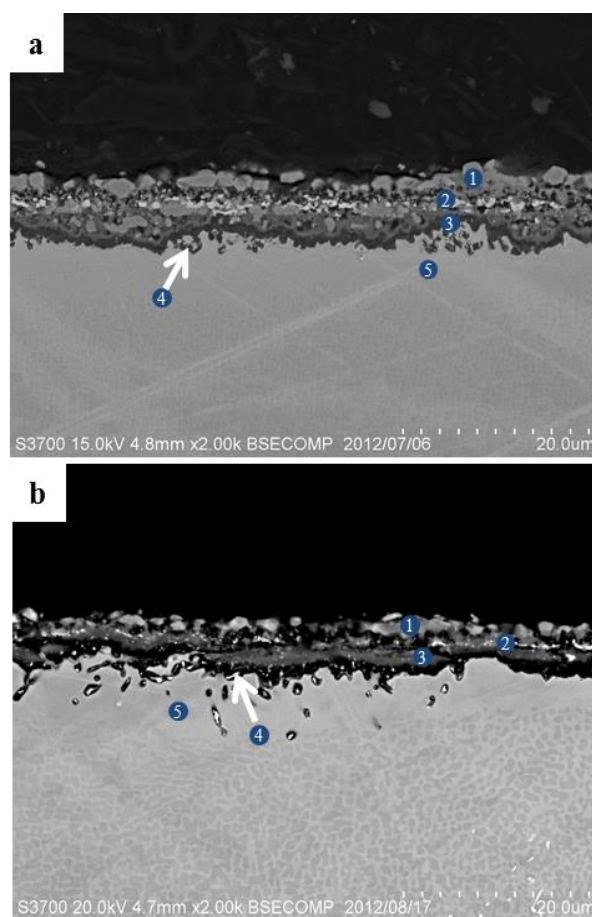

Figure 5. Cross-sectional SEM image of SC superalloy after 500 h oxidation at 1000°C: (a) (100) face and (b) (110) face. The chemical compositions of points 1-5 derived from EDS analysis for both orientations are presented in Table 2.

For the specimen with (100) face (Fig. 5a), the intermediate layer can be partitioned into two layers, the first intermediate layer mainly composed of $(Ni,Co)Al_2O_4$ and $CrTaO_4$ combined with $NiCr_2O_4$ and some small amounts of $NiTiO_3$ and $W_{20}O_{58}$. Whereas the second intermediate layer predominantly consisted of $(Ni,Co)Al_2O_4$ with less amount of $NiCr_2O_4$ (point 3). Meanwhile the specimen with (110) face (Fig. 5b), the first intermediate layer predominantly consisted of $CrTaO_4$ and $(Ni,Co)Al_2O_4$ combined with $NiCr_2O_4$ and some small amounts of $NiTiO_3$ and $W_{20}O_{58}$ (point 2).

Whereas the second intermediate layer predominantly composed of $(Ni,Co)Al_2O_4$ followed by $NiCr_2O_4$, $CrTaO_4$ and some small amount of $NiTiO_3$ and $W_{20}O_{58}$ (Fig. 8b).

The EDS results of the specimens after oxidation for 500 h at 1000 °C for both orientations were summarized in Table 2. Moreover, thickness of oxide scale increased to be approximately 5.2-10.8 μm on the (100) face and 3.7-6.9 μm on the (110) face after oxidation for 500 h (Fig. 5). From our observation, the EDS results were consistent with the XRD results obtained. The difference in thickness of oxide scale also indicated that the anisotropy on oxidation behavior occurred at 1000°C. This is one of indicator that the crystallographic orientation affected the oxidation behavior of SC superalloy.

Table 2. Chemical content of main elements in typical phase zone after 500 h oxidation at 1000°C (at.%) in Fig. 5.

Condition	Points of no.	Element content (at.%)										Note
		O	Ni	Al	Cr	Co	Ti	W	Ta	Hf	Re	
1000°C/500 h on the (100) face (Fig. 5a)	1	43.95	51.56	-	0.58	3.91	-	-	-	-	-	NiO+CoO
	2	46.02	21.06	5.06	10.3	5.79	3.13	1.85	6.79	-	-	$(Ni,Co)Al_2O_4+NiCr_2O_4+CrTaO_4+NiTiO_3+W_{20}O_{58}$
	3	48.94	11.53	35.24	1.84	2.45	-	-	-	-	-	$(Ni,Co)Al_2O_4+NiCr_2O_4$
	4	34.76	11.05	46.14	1.02	1.96	-	0.02	-	5.05	-	α-$Al_2O_3+HfO_2$
	5	-	70.23	3.05	8.4	13.5	0.23	2.94	0.19	-	1.14	Poor Al-zone
1000°C/500 h on the (110) face (Fig. 5b)	1	46.25	49.15	-	0.35	4.25	-	-	-	-	-	NiO+CoO
	2	38.51	17.16	4.57	24	10	2.4	0.35	3	-	-	$(Ni,Co)Al_2O_4+NiCr_2O_4+CrTaO_4+NiTiO_3+W_{20}O_{58}$
	3	41.92	18.38	20.72	7.18	5.61	4.02	0.63	1.54	-	-	$(Ni,Co)Al_2O_4+NiCr_2O_4+CrTaO_4+NiTiO_3+W_{20}O_{58}$
	4	32.17	7.23	56.33	0.41	0.84	-	-	-	3.02	-	α-$Al_2O_3+HfO_2$
	5	-	66.04	3.05	11.73	14.31	0.73	2.78	0.26	-	1.09	Poor Al-zone

4. DISCUSSION

The oxidation kinetics of SC superalloys follows the parabolic law between the temperatures of 800 °C and 1100 °C [15]. The oxidation kinetics showed that the specimens with (100) face oxidized at rates more rapid than those of (110) face (Fig. 1). The oxidation kinetics of SC superalloy in this paper nearly follows the parabolic law [15,16]. It confirmed that the anisotropy occurred not only in the mechanical properties but also on the oxidation behavior [8] of SC metals.

To our understanding, the simple oxides such as NiO, CoO, Al_2O_3 and others are normally formed during initial oxidation stage. Then, continued with the formation of a mixed-oxide scale on the surface of SC superalloy after 500 h oxidation at 1000 °C. The interaction of the solid phase among the simple oxides led to the formation of spinels $(Ni,Co)Al_2O_4$ [17], $NiCr_2O_4$ [18], $NiTiO_3$ [5] and a complex oxide $CrTaO_4$ [19]. After the mixed-oxide scale formed, the activity of oxygen at the scale/SC superalloy interface may decrease which mitigates the selective oxidation of Al, bringing on the formation of more α-Al_2O_3. With increasing oxidation time, the inner α-Al_2O_3 layer grew laterally and converted to form of a compact inner scale at the end. After 500 h oxidation, the inner layer becomes thick due to the continuous diffusion of both Al and O. However, some isolated HfO_2

precipitates were observed in the present study. The HfO_2 precipitates [20] were resulted from the reaction of $HfC + O_2 \rightarrow HfO_2 + CO_2$. These precipitates developed through the outward diffusion of hafnium from the substrate to the oxide layer. The concentration of HfO_2 precipitates was given in Table 2.

The transient-oxidation period was very short during oxidation at 1000 °C. This is due to the rapid formation of the inner α-Al_2O_3 resulting from swift outward diffusion of Al in the superalloy. Therefore, Ni diffusion outward is intercepted by the rapid development of the inner α-Al_2O_3 layer, and NiO growth is lastly impeded. Cr_2O_3 could be formed during the early stage of oxidation but it was not observed after 500 h oxidation at 1000 °C. This is likely owing to the effect of continuous oxidation of Cr_2O_3 (s) to CrO_3 (g) at high temperatures [21]. Besides, the thin $CrTaO_4$-rich complex oxide layer was found on both surfaces (Fig. 5). However, the thin $CrTaO_4$-rich complex oxide layer seemed not to be continued in some regions on the (110) face (Fig. 5b). This could be attributed to the rapid formation of a continuous α-Al_2O_3 inner layer at high temperatures which slowed the rate of oxide down considerably owing to the slow diffusion of reactive species in α-Al_2O_3. Hence, the growth of $CrTaO_4$ and other oxides is impeded on the (110) face.

The present results revealed more rapid oxidation rate on the (100) face than that on the (110) face [22,23]. The difference in oxidation rate constant (k_p) values between the two surfaces led to the difference in NiO grain size, oxides scale structure and thickness of oxide scale. Indeed, these differences were evidence for the anisotropic oxidation resistance. The difference in oxidation rates between the two surface orientations could be attributed to a grain size effect. An increase in the grain size of NiO at the surface related to an increase in the available paths for ion transport as reported elsewhere [9,24,25]. Therefore, various oxidation rates resulted from the different surface of the specimen will influence the grain size, oxide scale phases formed as well as its thickness during oxidation. The different oxide scale phase constitution in the intermediate layer between the two surfaces is presented in Table 2. Moreover, the maximum thickness of the oxide scale formed was approximately 10.8 μm on the (100) face and 6.9 μm on the (110) face after oxidation for 500 h at 1000°C (Fig. 5).

Previous work, Herchl et al. studied that the specimens having (100)-oriented oxidized more rapidly than the (110) and (111)-oriented specimens in SC nickel [26]. Moreover, Schuh et al. also investigated that the oxidation rate of the oriented specimens was increased in the order of (001) > (011) > (111) in SC nickel [27]. In fact, the present results obtained are consistent with the previous works [26,27]. Basically, the formation of the oxide scales on the surfaces of SC nickel containing a large number of short-circuit diffusion paths, where these short-circuit diffusion paths play an important role during oxidation in the single crystal surfaces as a function of the crystallographic orientations [28]. They often occurred due to the dependent epitaxial-growth force (stress) of the oxide scale on the surface of SC superalloys during oxidation. From this sense, it can be understood that the specimens with different crystallographic orientations could have various oxidation rates. Furthermore, the generation of growth stresses within the oxide scale as the oxidation reaction progresses has been proposed by Mrowec as a dissociative mechanism [29]. The growth stresses arise in the oxide scale, since the oxide scale must relax to maintain contact with the substrate when cations are mobile. However, it is still not well-understood the mechanism of the anisotropic oxidation resistance in Ni-

base SC superalloys. It is thus considered that the difference in oxidation rate should have to be taken into consideration as the main reason for the anisotropy phenomenon. Its differences may be due to the different structure of γ/γ′ interface between the two orientations of the specimens was found (Fig. 3). It has been explained formerly that SC superalloys are particularly consisted of γ′ and γ phases. SC superalloys are strengthened by the cuboidal γ′ precipitates that uniformly distributed in the γ matrix [1-3]. The different surface orientations of the specimens lead to the interfacial structure of the phase boundaries between γ′ and γ phases is also different. The schematic illustration of the interfacial structure of the phase boundaries between γ′ and γ phases of the two surfaces is shown in Fig. 6.
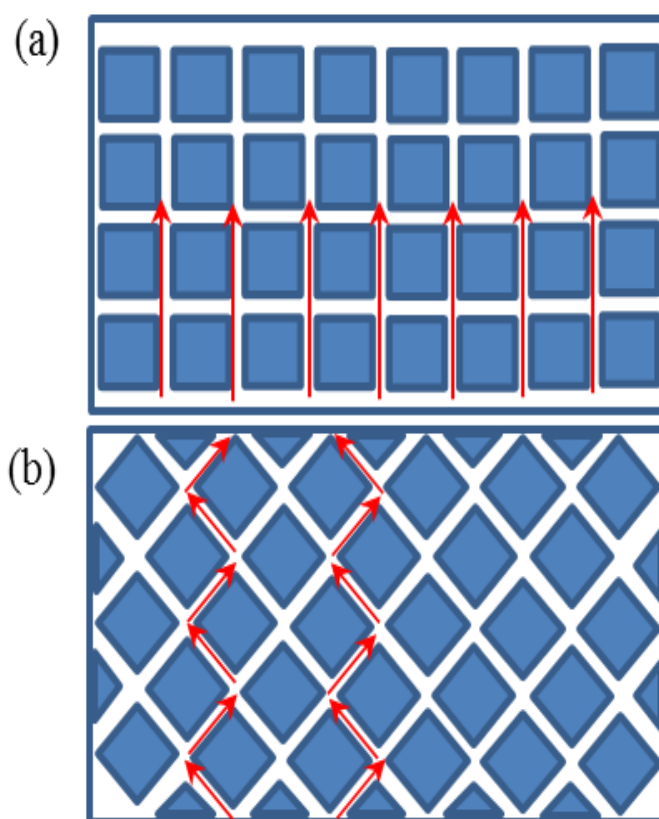

Figure 6. Schematic illustration of the interfacial structure of the phase boundaries between γ′ and γ phases: (a) (100) face and (b) (110) face. (Note that the rapid diffusion paths of cations during oxidation indicated by red arrows).

The phase boundaries are perpendicular to the external surfaces in the specimens with (100) face. Whereas in the specimens with (110) face, the phase boundaries make an angle of 45° to the external surfaces. Note that the oxide scales grow epitaxially with reference to the substrate surface during the initial oxidation stage, but after sometimes the transition of the epitaxial-oxide scale to randomly-oriented oxide scale take places. As can be showed in Fig. 6, the boundaries between the γ′ and γ phases could act as diffusion paths for cations diffusion during oxidation. For the specimens with (100) face, the rapid diffusion paths go through the boundaries smoothly without any obstacle as indicated by the red arrows (Fig. 6a). In the other words, the rapid paths for element diffusion represents as the straight line paths on the (100) face. Whereas for the specimens with (110) face, the

diffusion paths appears as the zig-zag paths as indicated by the red arrows (Fig. 6b). Note that after 500 h oxidation, the concentration of Al at the oxide scale/substate interface between the surfaces is distinct as indicated in point 4 in Table 2. It is shown that the (110) face had a higher Al concentration than that of (100) surface, this indicates that the difference in oxidation rate may be controlled by the Al outward diffusion from substrate to oxide scale/substrate interface. The thickness of the inner α-Al_2O_3 layer between the two surfaces after 500 h oxidation is somewhat different where the average thickness of its layer was about 2.14 μm on the (110) face and 1.76 μm on the (100) face (Fig. 5).

5. CONCLUSION

The anisotropic oxidation resistance in a SC superalloy has been investigated at 1000 °C for 500 h. The results showed that the specimens with (100) face had a higher oxidation rate than the specimens with (110) face. It indicated that the anisotropy on oxidation resistance occurred between the two orientations. The anisotropic oxidation resistance can be easily recognized from the difference in NiO grain size, oxides scale structure and thickness of oxide scale. It is considered the anisotropic oxidation behavior was due to the different structure of γ/γ′ interface with respect to the surface orientations of the specimens. Therefore, the boundaries between the γ′ and γ phases could act as rapid diffusion paths for cations diffusion during oxidation. Finally, the difference in rapid diffusion paths resulted in the difference in oxidation rate between the two specimen orientations.

References

1. D.W. MacLachlan, D.M. Knowles, *Mater. Sci. Eng*. A 302 (2001) 275.
2. J.S. Bae, J.H. Lee, Kim SS, Jo CY, *Script. Mater*. 45 (2001) 503.
3. K. Shirvani, M. Saremi, A. Nishikata, T. Tsuru, *Corros. Sci.* 45 (2003) 1011.
4. B. Pieraggi, F. Dabosi, *Mater. Corros*. 38 (1987) 584.
5. M.H. Li, X.F. Sun, T. Jin, H.R. Guan, Z.Q. Hu, *Oxid. Met*. 60 (2003) 195.
6. N. Czech, F. Schmitz, W. Stamm, *Surf. Coat. Technol*. 68-69 (1994) 17.
7. M.B. Henderson and J.W. Martin, *Acta Mater*. 44 (1996) 111.
8. V. Sass, U. Glatzel, and M. Feller-Kniepmeier, *Acta Mater*. 44 (1996) 1967.
9. N.N. Khoi, WW. Smeltzer, and J.D. Embury, *J. Electrochem. Soc*. 122 (1975) 1495.
10. J. Doychak, J.L. Smialek, and T.E. Mitchell, *Metall. Trans*. A 20 (1989) 499.
11. F.H. Yuan, E.H. Han, C.Y. Jo, T.F. Li and Z.Q. Hu, *Oxid. Met*. 60 (2003) 211.
12. B. Wang, C. Sun, J. Gong, R. Huang, L. Wen, *Corros. Sci*. 46 (2004) 519.
13. C.Y. Bai, Y.J. Luo, C.H. Koo, *Surf. Coat. Technol*. 183 (2004) 74.
14. G. Calvarin, A.M. Huntz, R. Molins, *Mater. High Temp*.17 (2000) 257.

15. T.F. An, H.R. Guan, X.F. Sun and Z.Q. Hu, *Oxid. Met*. 54 (2000) 301.
16. J. Huang, H. Fang, X. Fu, F. Huang, H. Wan, Q. Zhang, S. Deng, and J. Zu, *Oxid. Met*. 53 (2000) 273.
17. B. Pieraggi, *Mater. Sci. Eng*. 88 (1987) 199.
18. H.M. Hindam, W.W. Smeltzer, *J. Electrochem. Soc.* 127 (1980) 1622.
19. C.T. Liu, X.F. Sun, H.R. Guan, Z.Q. Hu, *Surf. Coat. Technol*. 197 (2005) 39.
20. H. Tamaki, A. Okayama, B. Onay, A. Yoshinari, Effect of solution treatment on the hot corrosion resistance of a second generation DS superalloy, In : J. Lecomte-Beckers, M. Carton, F. Schubert and P. J. Ennis (Eds.), Materials for Advanced Power Engineering 2002, The 7th Liege Conference, Universite De Liege, Belgium, 2002, pp. 1205-1215.
21. D. Caplan and M. Cohen, *J. Electrochem. Soc*. 108 (1961) 438.
22. F.W. Young, Jr, J.V. Cathcart, A.T. Gwathmey, *Acta Metall*. 4 (1956) 145.
23. C.A. Schuh, K. Anderson, C. Orme, *Surf. Sci*. 544 (2003) 183.
24. F. Czerwinski, J.A. Szpunar, *Corros. Sci*. 41 (1999) 729.
25. D. Monceau, B. Pieraggi, *Oxid. Met*. 50 (1998) 477.